Solar Energy Materials & Solar Cells 144 (2016) 684–690

Contents lists available at ScienceDirect

Solar Energy Materials & Solar Cells

journal homepage: www.elsevier.com/locate/solmat

Deposition temperature induced conduction band changes in zinc tin oxide buffer layers for Cu(In,Ga)Se_2 solar cells

Johan Lindahl *, Jan Keller, Olivier Donzel-Gargand, Piotr Szaniawski, Marika Edoff, Tobias Törndahl

Ångström Solar Center, Division of Solid State Electronics, Uppsala University, P. O. Box 534, SE-75121 Uppsala, Sweden

ARTICLE INFO

Article history:
Received 10 June 2015
Received in revised form
14 September 2015
Accepted 26 September 2015
Available online 11 November 2015

Keywords:
Zinc tin oxide (ZTO)
Atomic layer deposition (ALD)
Buffer layer
Thin film photovoltaics
CIGS
Conduction band line-up

ABSTRACT

Thin film Cu(In,Ga)Se_2 solar cells with ALD-deposited $Zn_{1-x}Sn_xO_y$ buffer layers are fabricated and the solar cell properties are investigated for varying ALD deposition temperatures in the range from 90 °C up to 180 °C. It is found that a process window exists between 105 °C and 135 °C, where high solar cell efficiency can be achieved. At lower ALD deposition temperatures the solar cell performance is mainly limited by low fill factor and at higher temperatures by low open circuit voltage. Numerical simulations and electrical characterization are used to relate the changes in solar cell performance as a function of ALD deposition temperature to changes in the conduction band energy level of the $Zn_{1-x}Sn_xO_y$ buffer layer. The $Zn_{1-x}Sn_xO_y$ films contain small ZnO or ZnO(Sn) crystallites (< 10 nm), which may lead to quantum confinement effects influencing the optical band gap of the buffer layer. The ALD deposition temperature affects the size of these crystallites and it is concluded that most of the changes in the ZTO band gap occur in the conduction band level.

1. Introduction

Cu(In,Ga)Se_2 (CIGS) is a proven absorber material for making high efficiency photovoltaic devices. A standard CIGS solar cell consists of a glass/Mo/CIGS/buffer layer/i-ZnO/ZnO:Al stack. In this stack the role of the buffer layer is to ensure good electrical and optical interface properties between the CIGS absorber and the ZnO layers, and therefore the buffer layer plays a decisive role in the performance of the solar cell. To obtain adequate charge carrier transport, the buffer layer should establish a suitable energy band line-up to both the absorber and the front electrode [1]. It is also beneficial for the position of the Fermi level to be located close to the absorber conduction band edge at the absorber/buffer interface (type inversion) in order to mitigate the detrimental effects of possible interface defects [2]. Furthermore, the band gap energy (E_g) of the buffer layer material should be as high as possible to reduce parasitic optical absorption.

The historically most common buffer layer in CIGS solar cells is cadmium sulfide, CdS, deposited by chemical bath deposition (CBD). However, both this material and the deposition technique have some drawbacks. One disadvantage is the low direct band gap of CdS, 2.4–2.5 eV [3], which causes parasitic absorption in the low wavelength regime. Another downside is that the CBD technique is a non-vacuum method, while usually both the absorber and the ZnO layers are deposited by vacuum based techniques. This makes CBD unfavorable for industrial processing. Furthermore, cadmium is classified as toxic and carcinogenic [4].

Development of alternative buffer layer materials and the use of deposition techniques other than CBD are therefore major research topics [5,6]. One proven vacuum technique for deposition of alternative buffer layers is atomic layer deposition (ALD) [7]. ALD is a chemical vapor deposition technique that employs alternating self-limiting sequential gas-to-solid reactions, which enables highly controllable deposition of uniform and conformal films at relatively low temperatures [8].

Zinc tin oxide, $Zn_{1-x}Sn_xO_y$ (ZTO), is a wide band gap semiconductor material that has shown potential as a buffer layer in several thin film solar cell techniques. ZTO record conversion efficiencies of 18.2% for CIGS [9] and 2.7% for Cu_2O [10] solar cells have been achieved with ALD, and 16.5% for CdTe [11] solar cells with RF magnetron sputtering. ALD-deposited ZTO demonstrates uniform and conformal growth at a linear rate of about 0.4 Å/cycle on both glass and CIGS, although a lower initial growth rate has been observed on CIGS. About 15 nm thin ZTO buffer layers are sufficient to fabricate highly efficient CIGS solar cells [12]. ALD ZTO has been characterized in several publications and it has been

* Correspondence to: Uppsala University, Department of Engineering Sciences, Solid State Electronics, Box 534, SE-751 21 Uppsala, Sweden. Tel.: +46 18 471 7239.
E-mail address: johan.lindahl@angstrom.uu.se (J. Lindahl).

http://dx.doi.org/10.1016/j.solmat.2015.09.048

found that the band gap of the material has a non-trivial dependence on the zinc-to-tin ratio [10,13,14].

The band alignment at the buffer/absorber interface in a CIGS solar cell strongly affects the performance. A negative conduction band offset (CBO), $\chi_{absorber}-\chi_{buffer}<0$, usually referred to as a cliff, is undesirable because it reduces the type inversion close to the interface and leads to increased recombination via interface states and thereby V_{oc} and FF losses [1,2,15]. A positive CBO, $\chi_{absorber}-\chi_{buffer}>0$, usually referred to as a spike, may lead to a barrier that blocks photo-generated electrons in the absorber from entering the depletion region under forward bias conditions and can have a detrimental effect on J_{sc} and FF [1,16]. However, a moderate spike does not limit current collection and is therefore desirable [1]. It has been shown that it is possible to change the conduction band energy level of ZTO, by changing the composition, and match it with the conduction band energy level of solar cell absorber materials [10,13] so that a favorable CBO and good solar cell performance can be achieved [17,18].

In a previous publication it was shown that the band gap of ZTO films decreases with increasing deposition temperature even if the composition stays the same [19]. The possible reason for this is that the ALD-deposited ZTO films contain ZnO or ZnO(Sn) crystallites in the nanometer range. These crystallites are small enough to give rise to quantum confinement effects, which increases the band gap energy. When the deposition temperature and/or the zinc content are increased these crystallites increase in size, which results in films a lower effective band gaps. In this study, ZTO films with the same composition and thickness, but deposited at varying ALD temperatures, are grown on CIGS as buffer layers and the CIGS solar cell performance is evaluated.

2. Material and methods

2.1. Sample fabrication

The CIGS solar cells investigated in this study are manufactured with the Ångström Solar Center baseline processes [9] with exception for the CIGS layers. Instead the CIGS is co-evaporated in a batch reactor with open-boat Cu, In and Ga sources [20]. Prior to the buffer layer deposition, the CIGS layers are etched for 1 min in a 5 wt% KCN solution.

The ZTO buffer layer is deposited in a Microchemistry F-120 ALD reactor using the same process and parameters as summarized in [19]. The deposition temperature of the ZTO films is varied between 90 °C and 180 °C in this study and the resulting material parameters are summarized in Table 1. ZTO buffer layers deposited by ALD at 120 °C are proven to be conformal and have a uniform depth composition on CIGS [12]. The thickness of the ZTO buffer layers affects the solar cell performance [12] and the thickness of ZTO films depends on the deposition temperature [19]. The number of pulse cycles is therefore adjusted to obtain ZTO films with similar thickness. It should be clarified that the material parameters of the ZTO films in Table 1 are measured when deposited directly on glass and that the EDS scans performed in this paper show that the thickness of the ZTO films grown on CIGS is roughly 10 nm thinner than ZTO films grown on glass (measured by x-ray reflectivity). This is the same finding as has previously been observed in [12], and is due to longer nucleation times for ZTO on CIGS as compared to on glass.

Table 1
ZTO buffer layer deposition and resulting material parameters on glass substrates.

Deposition temperature [°C]	Number of ALD pulse cycles	[Sn]/([Sn]+[Zn]) composition	Thickness [nm]	Density [g/cm^3]	Indirect band gap [eV]
90	1600	0.185	53	3.9	3.74[a]
105	1200	0.175	48	4.2	3.62[b]
120	1100	0.169	50	4.3	3.49[a]
135	1000	0.176	54	4.5	3.43[b]
150	1000	0.172	55	4.6	3.35[a]
165	1000	0.173	58	4.8	3.29[b]
180	1000	0.172	56	4.7	3.23[a]

[a] Band gaps from indirect Tauc plot models measured by ellipsometry [19].
[b] Interpolated values.

As described more in detail in previous work [19], the [Sn]/([Sn]+[Zn]) composition of the films is controlled by the relative number of zinc- or tin-containing precursor pulses. The pulse sequence is kept constant with three Zn-precursor:N_2:H_2O:N_2 cycles for every two Sn-precursor:N_2:H_2O:N_2 cycles, which resulted in a process with a Sn/(Sn+Zn) cycle fraction of 0.4. The final composition of the films differs from the cycle fraction due to differences in reactive sites as well as different sizes of the precursor molecules. The [Sn]/([Sn]+[Zn]) composition of the ZTO buffer layers affects the solar cell performance [18] and is measured by X-ray fluorescence spectrometry (XRF). However, the composition is only marginally influenced by the deposition temperature, as Table 1 shows. Moreover, the ZTO buffer layers used in the investigated solar cell samples are deposited in the same run as the glass samples used for material and optical characterization, and should therefore have similar properties. The indirect band gap of ZTO, as measured by ellipsometry, and extracted by indirect Tauc plot models [21], is found to vary from 3.74 eV at 90 °C to 3.23 eV at 180 °C.

2.2. Characterization methods

The transmission electron microscopy (TEM) analyses are done on a FEI Tecnai F30 ST TEM with an acceleration voltage of 300 kV. The X-ray energy-dispersive spectroscopy (XEDS) is carried out in scanning mode, with a scan step of 2.5 nm. The analysis area of the CIGS–ZTO interface is chosen to be parallel to the electron beam. The intensity profiles are obtained by peak integration from the background corrected EDS maps. For all elements the K-line is used. The thickness of the ZTO buffer layer is measured from the image intensity profiles. The TEM electron transparent lamellae is prepared using the in-situ lift-out method described elsewhere [22].

A certified ORIEL Sol2A solar simulator from Newport Stratford Inc. is used for the current density–voltage (J–V) measurements, giving short circuit current density (J_{sc}), open circuit voltage (V_{oc}), fill factor (FF) and conversion efficiency (η). External quantum efficiency (EQE) measurements are used to correct the mismatch between the spectrum of the ORIEL Sol2A lamp and the AM 1.5 spectrum to acquire correct J_{sc} values. To obtain the same J_{sc} values for the J–V measurements, as extracted from the EQE measurements, the intensity of the Sol2A solar simulator is adjusted. An in-house system, similar to the measurement setup presented in [23], is used for the EQE measurements. For both measurements the samples are kept at 25 °C by Peltier elements and the samples are measured without any preconditioning. Because there are multiple individual solar cells on each sample, unintentional light soaking might occur during the J–V measurements before all cells are measured on a given sample.

Temperature-dependent J–V measurements are performed in a cryostat-based setup with the sample stage cooled by liquid N_2. The sample temperature is monitored and controlled by a Lake Shore 330 unit, and the J–V characteristics are measured by a Keithley 2401 SourceMeter. Illumination is provided by a white LED with a narrow energy distribution around 445 nm and a wide distribution between 490 nm and 700 nm. The light intensity is

Table 2
Material parameters used for the simulation in SCAPS-1D.

Property	CIGS	CIGS/ZTO interface	ZTO	i-ZnO	ZnO:Al
Thickness [nm]	1700	–	50	80	350
Band gap [eV]	1.15	–	3.20–3.74	3.30	3.40
Electron affinity [eV]	4.5	–	4.60–4.06	4.55	4.55
Doping density [1/cm^3]	1×10^{16} (A)	–	1×10^{17} (D)	1×10^{17} (D)	1×10^{20} (D)
Defect density [1/cm^3]	2×10^{15} (N)	–	1×10^{17} (N)	–	–
Capture cross section [cm^2]	1×10^{-14}	–	1×10^{-11}	–	–
Interface defect concentration [1/cm^2]	–	1×10^{10}	–	–	–

(A) Acceptor type defect/doping.
(D) Donor type defect/doping.
(N) Neutral type defect.

Table 3
Average *J–V* parameters of 12 cells and standard deviation for samples where the $Zn_{1-x}Sn_xO_y$ buffer layer is deposited at different temperatures.

Deposition temp. [°C]	V_{oc} [mV]	J_{sc} [mA/cm^2]	FF [%]	η [%]
90	632 ± 7	36.4 ± 0.3	37.2 ± 3	8.5 ± 0.8
105	672 ± 10	35.6 ± 0.3	74.5 ± 0.4	17.8 ± 0.3
120	662 ± 9	36.3 ± 0.3	73.2 ± 1	17.6 ± 0.4
135	642 ± 3	38.5 ± 0.4	72.4 ± 0.3	17.9 ± 0.2
150	637 ± 6	35.7 ± 0.4	70.3 ± 0.9	16.0 ± 0.3
165	607 ± 10	35.0 ± 1	60.9 ± 8	13.0 ± 2
180	549 ± 20	35.2 ± 0.4	62.5 ± 2	11.9 ± 0.8
CdS ref	681 ± 4	35.2 ± 0.3	74.6 ± 0.6	17.9 ± 0.2

calibrated to give J_{sc} within 10% of the value at AM 1.5 spectrum illumination.

2.3. Numerical simulation

In order to understand and explain the measured *J–V* characteristics, numerical simulations are performed by employing the one-dimensional device simulation tool SCAPS-1D [24]. The important material parameters used to model the CIGS/ZTO solar cells are summarized in Table 2. Since the simulations mainly focuses on qualitative effects of varying band alignments at the buffer interfaces (CIGS/ZTO and ZTO/i-ZnO), the bulk properties are kept as simple as possible (e.g. no Ga/In grading is applied even if the actual samples have linear grading). The constant band gap of the absorber is set to $E_g=1.15$ eV, which is in good agreement with the value expected at the hetero-interface based on EQE-curves (not shown here) for the investigated samples. The corresponding electron affinity (χ) is assumed to be $\chi=4.5$ eV [25]. A neutral deep defect at $E_g/2$ is added in the bulk of the CIGS layer, tuned to the obtained V_{oc} values, leading to a minority carrier diffusion length of 800 nm. For ZTO with $E_g=3.2$ eV an electron affinity of $\chi=4.6$ eV is assumed. The incoherent absorber/buffer interface is modeled by introducing interface defects, while the electronic parameters of the other layers are chosen as best guesses based on earlier studies.

3. Results

3.1. Solar cell performance

Table 3 summarizes how the *J–V* parameters of complete solar cells with ZTO buffer layers are affected by the ALD deposition temperature. Fig. 1(a) illustrates the *J–V* curves for the top cells of the samples with the ZTO buffer layer deposited at 90 °C, 120 °C, 150 °C and 180 °C. The intermediate temperatures are neglected here to illustrate the trend more clearly. The material properties of the corresponding ZTO films on glass are presented in Table 1 and more in detail in [19]. Table 3 and Fig. 1(a) show that J_{sc} is not significantly affected by the deposition temperature. The 135 °C sample is an outlier with approximately 3 mA/cm^2 higher J_{sc} than the rest of the samples. However, EQE curves and XRF-measurements of the CIGS layer (not shown here) have revealed that this is due to a slightly different CIGS composition in this sample as compared with the other samples. A composition more in-line with the other samples is assumed to yield a lower J_{sc} and higher V_{oc} for two reasons, the first being the lower band gap of the CIGS, and the second the difference in band offset. At a deposition temperature of 90 °C the conversion efficiency is mainly limited by a lower FF, which is due to a roll-over blocking behavior observed in Fig. 1(a). The V_{oc} is highest at 105 °C and then decreases with increasing temperature, whereas the fill factor also drops at higher temperatures.

Analysis of the temperature dependence of V_{oc} is a way to characterize the recombination mechanisms that limit the performance of solar cells. In Fig. 2 the thermal evolution of V_{oc} in the 100–330 K range is plotted for representative devices with ZTO buffers deposited at different temperatures. The $T=0$ K intercept, extrapolated from the linear regime around 300 K, is the activation energy (E_A) of the dark saturation current J_0 and is related to the dominant recombination mechanism [26]. Extrapolating V_{oc} ($T\rightarrow$ 0 K) results in 1.1 and 1.13 V for the samples where the ZTO buffer layers are deposited at 120 °C and 150 °C, respectively. The values of E_A for the samples with ZTO buffer layers deposited at 90 °C and 180 °C are obviously significantly lower.

3.2. Material and interface properties

HR-TEM images of one of the cells deposited at 120 °C and one of the cells deposited at 180 °C are taken to investigate if the ZTO buffer layer demonstrates the same structural properties when deposited on CIGS as compared to the glass substrates in [19]. It is found that the ZTO buffer layer is extremely beam sensitive as crystal growth is triggered by simple exposure to the electron beam. A few minutes are enough to crystallize the ZTO buffer layer completely. However, when the beam exposure is lowered to the strict minimum for a TEM image acquisition (15–20 s), the sample where the ZTO buffer layer is deposited at 120 °C shows only a few crystals with sizes below 3–4 nm, while the 180 °C sample demonstrates more crystals with a sizes around 5–7 nm. The results in [19] demonstrate that ALD ZTO films contain ZnO or ZnO (Sn) crystallites in the nanometer range, and that these increase in size when the deposition temperature and/or the zinc content increases. The results from the TEM investigations performed for this paper show that this also seems to be valid when ZTO is deposited on CIGS.

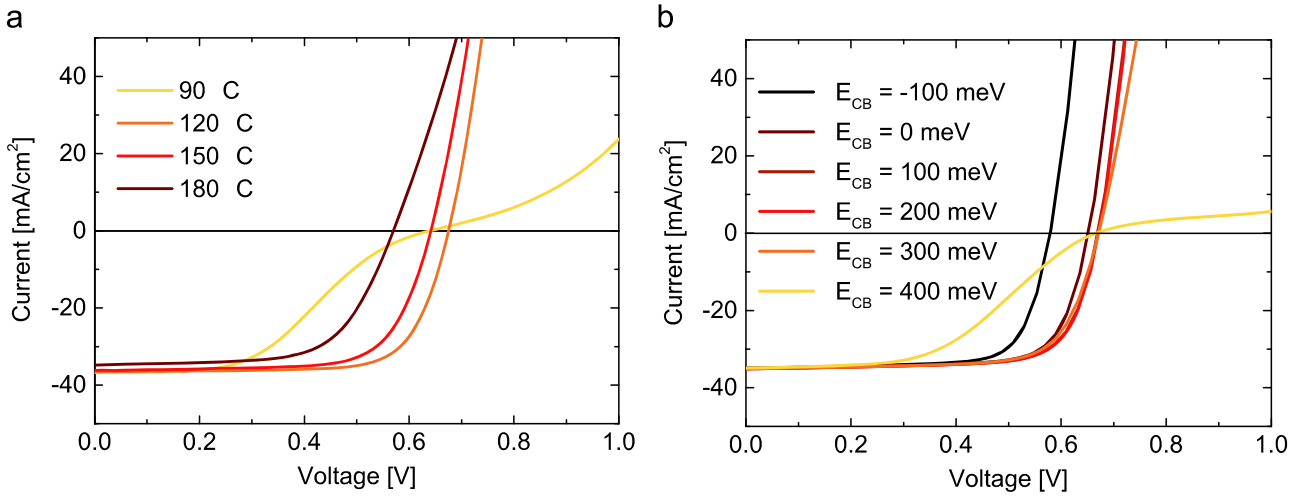

Fig. 1. (a) *J–V* curves of the best solar cells, out of 12 cells on each sample, where the ZTO buffer layer is deposited with a Sn/(Sn+Zn) cycle fraction of 0.4 at deposition temperatures of 90 °C, 120 °C, 150 °C and 180 °C. (b) Simulated *J–V* characteristics assuming different CIGS/ZTO conduction band offsets ΔE_{CB}.

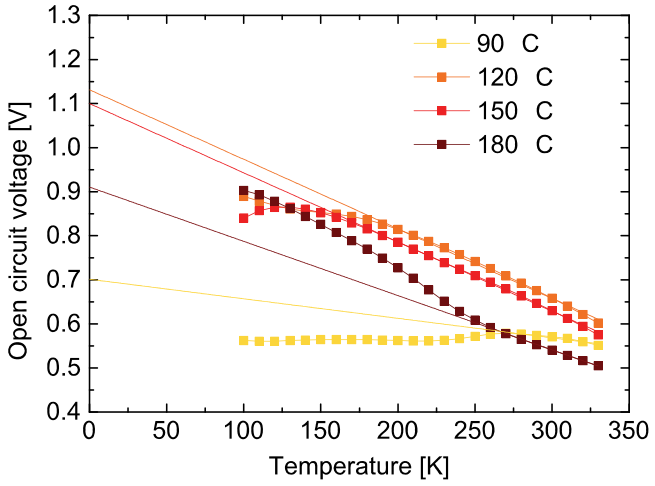

Fig. 2. Temperature dependence of V_{oc} of cells where the ZTO buffer layers are deposited with a Sn/(Sn+Zn) cycle fraction of 0.4 at deposition temperatures of 90 °C, 120 °C, 150 °C and 180 °C.

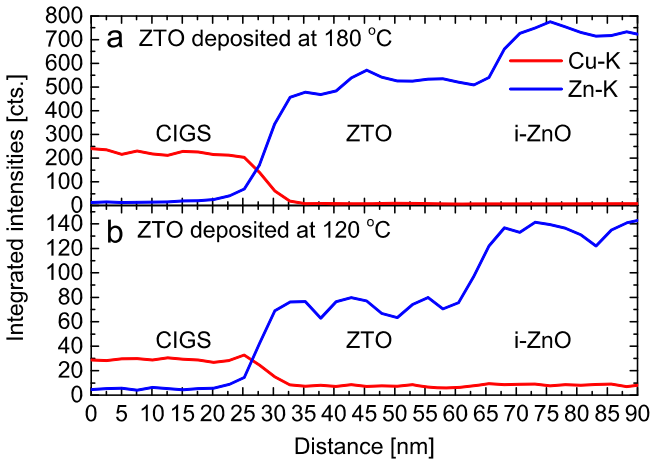

Fig. 3. EDS scans over the CIGS/ZTO interface, where the ZTO buffer layer is deposited by a Sn/(Sn+Zn) cycle fraction of 0.4. (a) The ZTO layer is deposited at 180 °C. (b) The ZTO layer is deposited at 120 °C.

To investigate if the deposition temperature influences the ZTO/CIGS interface, EDS scans of the 120 °C and 180 °C samples are performed. The counts of the K-peaks of Cu and Zn of the two scans are shown in Fig. 3. In and Sn are not included in the figure, because they have overlapping L-peaks. Ga is omitted due to Ga ions are used during the sample preparation, which leave traces in the sample. The difference in absolute intensities between the two scans is due to a shadowing effect from the sample holder that occurred in the scan of the 120 °C sample. Fig. 3 demonstrates that no diffusion of elements across the interface seems to occur in neither of the samples and that the interface is within 8 nm for both samples, which is in good agreement with the findings in [12]. This means that the influence of the deposition temperature on the inter-diffusion across the CIGS/ZTO interface is limited and should not influence the *J–V* parameters.

3.3. Simulated results

In an earlier work, the indirect band gap of ZTO was found to decrease from 3.74 eV at a deposition temperature of 90 °C to 3.23 eV at 180 °C [19]. It is of importance to know if the changes in E_g at different deposition temperatures are mainly related to changes in the conduction band energy, rather than in the valence band energy. To investigate this and to see if the changes in band gap can explain the obtained *J–V* characteristics, numerical simulations are performed. In this work, and in an earlier work [19], it is suggested that the ZTO films contain ZnO or ZnO(Sn) nanoparticles. Previously it has been shown that essentially all of the quantum size effects of pure-ZnO quantum dots manifest through a shift in the conduction band [27]. It is therefore assumed in the simulation analysis that the changes in E_g (experimentally achieved by different deposition temperatures) exclusively affects the conduction band energy level. This assumption couples the two parameters in a linear relation, $\chi = 7.8\ \text{eV} - E_g$. Thus, the E_g of ALD ZTO deposited at 180 °C ($E_g = 3.23$ eV) yields a negative (cliff) CBO of -0.07 eV to the absorber, while ZTO with $E_g \geq 3.3$ eV results in a positive (spike) CBO. This is schematically illustrated in Fig. 4(a) and two of the resulting band diagrams, in short circuit condition under illumination, are demonstrated in Fig. 4(b).

In Fig. 1(b) the simulated *J–V* characteristics for varying E_g and corresponding χ values of the ZTO layer are shown. Fig. 1(b) clearly illustrates that the highest conversion efficiencies are obtained for positive CBO between 0.1 and 0.3 eV. However, a too large spike, according to the simulations in Fig. 1(b), leads to a blocking behavior with major FF losses and a slight decrease in V_{oc}. On the other hand, negative CBO will result in a major loss in V_{oc}.

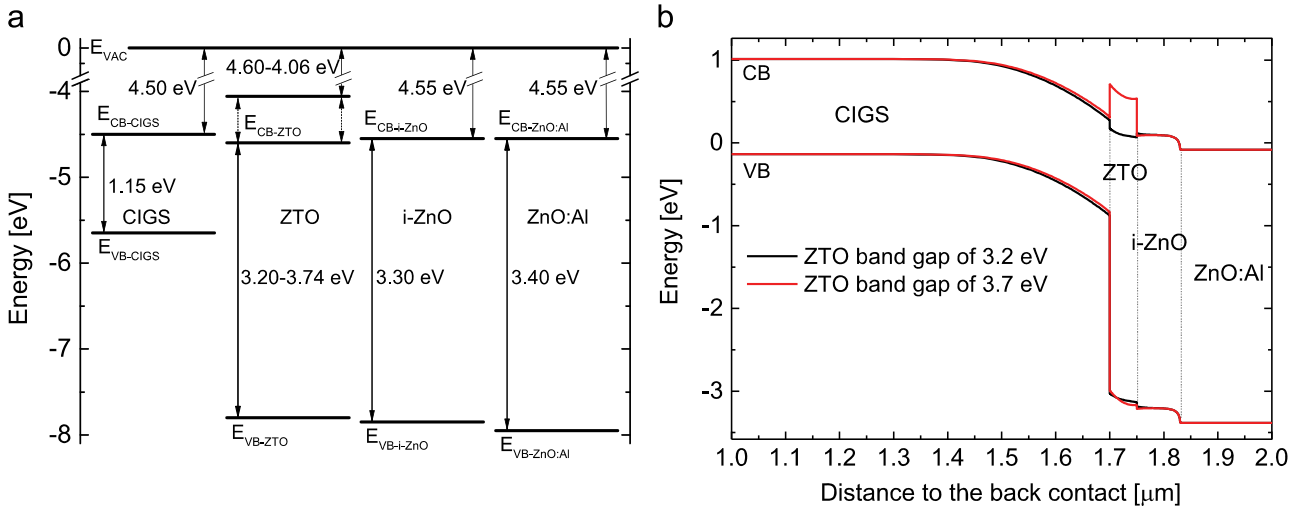

Fig. 4. (a) Schematic illustration of the band energy levels used in the SCAPS-1D simulations. (b) Zoomed in resulting band diagram for a simulated CIGS device with ZTO band gap of 3.2 eV and 3.7 eV at short circuit conditions.

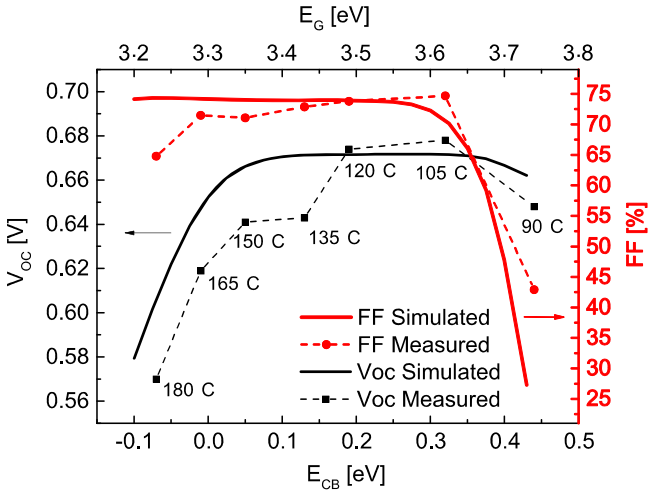

Fig. 5. Measured V_{oc} and FF values of best solar cells compared with numerically simulated V_{oc} and FF values, where the assumption is made that the band gap changes measured in [19] exclusively affect the conduction band position.

In Fig. 5 the measured V_{oc} and FF values of the best solar cells are plotted as a function of the band gap of ZTO extracted from Tauc plots generated from ellipsometry measurements [19]. Furthermore, these are compared with simulated V_{oc} and FF values, obtained under the assumption that all changes in the band gap energy occur in the conduction band. Therefore the *x*-axis shows the corresponding conduction band offset at the buffer/CIGS interface. It should be noted that the 135 °C sample is an outlier regarding CIGS composition and that a higher V_{oc} (more in line with the simulated values) is expected for this sample if the CIGS composition was similar to the rest of the samples.

4. Discussion

The *J*–*V* trends cannot be explained by changes in composition or by changes in the inter-diffusion across the CIGS/ZTO interface, since these material properties are not affected by the deposition temperature, as Table 1 and Fig. 3 show. Another possible explanation for the *J*–*V* trends is that the ALD deposition temperature influences the Na concentration in the CIGS close to the heterojunction. Studies have attributed roll-over *J*–*V* curves [28–31] and lower E_A [32] to Na deficiency in the absorber. However, it is unlikely that an ALD deposition temperature of 90 °C (or possibly above 150 °C) affects the Na content significantly, while all of the CdS reference samples as well as all the samples where the ALD deposition temperature is between 105 °C and 150 °C show normal behavior.

Rather, the qualitative match between the measured and simulated *J*–*V* curves in Fig. 1 and the corresponding values in Fig. 5 indicate that the *J*–*V* trends can be explained by the conduction band line-up theory. The results suggest that a majority of the band gap change observed in ZTO deposited at different temperatures occurs in the conduction band, which give rise to different conduction band offsets in the complete CIGS solar cell devices.

For the samples where the ZTO buffer layers are deposited at 120 °C and 150 °C, V_{oc} ($T \rightarrow 0$ K) $\approx E_g/q$, and E_A is therefore close to the absorber E_g at the interface (extracted from EQE measurements), which means that Shockley–Read–Hall recombination in the absorber bulk is the dominant recombination mechanism [26,33]. On the other hand, the values of E_A for the samples with ZTO buffer layers deposited at 90 °C and 180 °C are lower than the absorber E_g at the interface, indicating that interface recombination might be the dominant mechanism [15,34,35]. This strengthens the assumptions made and supports the simulated band diagram in Fig. 4(b). The increased interface recombination in the 180 °C sample can be explained by the negative CBO, which is associated with higher recombination rates via interface defects. The increased interface recombination in the 90 °C sample can be explained by that large spike CBO is formed in this sample. The theory says that such a spike under forward bias conditions blocks electrons at the CIGS/ZTO interface, which will have the consequence that the electron density at the interface is increased and this leads to increased recombination losses.

5. Outlook

It has previously been shown that varying the [Sn]/([Sn]+[Zn]) composition at a constant deposition temperature of 120 °C changes the band gap and conduction band edge position in a non-trivial way and that the highest conduction band edge position is obtained at a [Sn]/([Sn]+[Zn]) composition of approximately 0.2 [13]. The finding that the conduction band level of ZTO can be increased further by lowering the ALD deposition

temperature, while keeping the composition the same, opens up the possibility to establish suitable conduction band offsets to CIGS with interface E_g higher than the 1.15 eV used in this study. Increasing the Ga content in CIGS increases the band gap of the absorber, and nearly all of the variation in the band gap occurs in the conduction band [36]. In practice, it has been shown that V_{oc} increases proportionally to the absorber band gap, generally following the expression $V_{oc}=E_g/q-500$ mV [37,38] quite well. However, for the standard CIGS/CdS configuration, this proportional increase starts to decay at CIGS interface band gap energies higher than 1.3 eV, and consequently V_{oc} saturates around 0.8 V [16,37,38]. The reasons for the saturation of V_{oc} have been much debated, but one explanation is that the conduction band position of CdS is constant and that a negative CBO is formed when the minimum conduction band energy of CIGS increases, resulting in increased recombination through interface states.

Taking the solar AM 1.5 spectrum into account the highest theoretical conversion efficiencies, 32.8% and 33%, can be achieved by applying an absorber band gap energy of 1.15 eV or 1.35 eV, respectively [39]. The E_g at the buffer/absorber interface of the CIGS in this study is around 1.15 eV, which is close to the E_g of the first theoretical maxima and recent record CIGS solar cells [40]. The results in this study indicate that a small spike of 0.1 eV should be possible to achieve between CIGS with an interface band gap of 1.5 eV and a ZTO buffer layer with a [Sn]/([Sn]+[Zn]) composition of 0.18, resulting from an ALD deposition performed at 90 °C. Thus, the ZTO buffer layer opens up a possibility to investigate high band gap CIGS with absorber E_g close to the second theoretical maxima.

6. Conclusions

This study reports on how CIGS solar cell performance is affected by a variation of the deposition temperature of ALD grown zinc tin oxide (ZTO) buffer layers. It has previously been shown that the effect of the deposition temperature on the [Sn]/([Sn]+[Zn]) composition of ZTO films is small, while the band gap decreases with increasing deposition temperature. The changes are related to microstructural differences and transmission electron microscopy measurements have indicated that ZTO films contain small ZnO or ZnO(Sn) crystallites embedded in an amorphous matrix [19]. These crystallites are small enough for quantum confinement effects to occur and to influence the optical properties of ZTO. Comparing measured solar cell *J–V* parameters with simulated *J–V* characteristics indicates that a majority of the decrease in the band gap of ZTO with increasing deposition temperature occurs in the conduction band. At ALD deposition temperatures between 90 °C and approximately 135 °C these changes in conduction band level give rise to positive spike-like conduction band offsets between our CIGS and the ZTO buffer layer. The height of this transport barrier decreases with increasing deposition temperature. At 90 °C the spike is too high and a blocking behavior is observed, with large losses in FF and small losses in V_{oc} as a result. For deposition temperatures between 105 °C and approximately 135 °C a more favorable conduction band offset is formed, which leads to well-behaved solar cell characteristics with conversion efficiencies between 17.3% and 18.2%. At 150 °C a shift occurs as the V_{oc} starts to decrease, and at 165 °C the conduction band offset changes to a negative cliff-like CBO, with associated losses in V_{oc}. The results suggest that ZTO deposited at low temperatures could be a good buffer layer for high band gap CIGS.

Acknowledgment

The authors appreciatively acknowledge the Swedish Energy Agency (Grant no. 2012-004591), Sweden's innovation agency VINNOVA (Grant no. 2013-02199) and STandUP for the financial support.

References

[1] T. Minemoto, T. Matsui, H. Takakura, Y. Hamakawa, T. Negami, Y. Hashimoto, et al., Theoretical analysis of the effect of conduction band offset of window/CIS layers on performance of CIS solar cells using device simulation, Sol. Energy Mater. Sol. Cells 67 (2001) 83–88.
[2] R. Klenk, Characterisation and modelling of chalcopyrite solar cells, Thin Solid Films 387 (2001) 135–140.
[3] J.M. Doña, J. Herrero, Dependence of electro-optical properties on the deposition conditions of chemical bath deposited CdS thin films, J. Electrochem. Soc. 144 (1997) 4091–4098.
[4] M.P. Waalkes, Cadmium carcinogenesis in review, J. Inorg. Biochem. 79 (2000) 241–244.
[5] N. Naghavi, D. Abou-Ras, N. Allsop, N. Barreau, S. Bücheler, A. Ennaoui, et al., Buffer layers and transparent conducting oxides for chalcopyrite Cu(In,Ga)(S,Se)$_2$ based thin film photovoltaics: present status and current developments, Prog. Photovolt.: Res. Appl. 18 (2010) 411–433.
[6] W. Witte, S. Spiering, D. Hariskos, Substitution of the CdS buffer layer in CIGS thin-film solar cells, Vak. Forsch. Prax. 26 (2014) 23–27.
[7] J.A. van Delft, D. Garcia-Alonso, W.M.M. Kessels, Atomic layer deposition for photovoltaics: applications and prospects for solar cell manufacturing, Semicond. Sci. Technol. 27 (2012) 074002.
[8] R.L. Puurunen, Surface chemistry of atomic layer deposition: a case study for the trimethylaluminum/water process, J. Appl. Phys. 97 (2005) 121301.
[9] J. Lindahl, U. Zimmermann, P. Szaniawski, T. Törndahl, A. Hultqvist, P. Salomé, et al., Inline Cu(In,Ga)Se$_2$ co-evaporation for high-efficiency solar cells and modules, IEEE J. Photovolt. 3 (2013) 1100–1105.
[10] Y.S. Lee, J. Heo, S.C. Siah, J.P. Mailoa, R.E. Brandt, S.B. Kim, et al., Ultrathin amorphous zinc-tin-oxide buffer layer for enhancing heterojunction interface quality in metal-oxide solar cells, Energy Environ. Sci. 6 (2013) 2112–2118.
[11] X. Wu, High-efficiency polycrystalline CdTe thin-film solar cells, Sol. Energy 77 (2004) 803–814.
[12] J. Lindahl, J.T. Wätjen, A. Hultqvist, T. Ericson, M. Edoff, T. Törndahl, The effect of $Zn_{1-x}Sn_xO_y$ buffer layer thickness in 18.0% efficient Cd-free Cu(In,Ga)Se$_2$ solar cells, Prog. Photovolt. Res. Appl. 21 (2013) 1588–1597.
[13] M. Kapilashrami, C.X. Kronawitter, T. Törndahl, J. Lindahl, A. Hultqvist, W.-C. Wang, et al., Soft X-ray characterization of $Zn_{1-x}Sn_xO_y$ electronic structure for thin film photovoltaics, Phys. Chem. Chem. Phys. 14 (2012) 10154–10159.
[14] M.N. Mullings, C. Hägglund, S.F. Bent, Tin oxide atomic layer deposition from tetrakis(dimethylamino)tin and water, J. Vac. Sci. Technol. A: Vac. Surf. Films 31 (2013) 061503.
[15] M. Turcu, O. Pakma, U. Rau, Interdependence of absorber composition and recombination mechanism in Cu(In,Ga)(Se,S)$_2$ heterojunction solar cells, Appl. Phys. Lett. 80 (2002) 2598–2600.
[16] M. Gloeckler, J.R. Sites, Efficiency limitations for wide-band-gap chalcopyrite solar cells, Thin Solid Films 480–481 (2005) 241–245.
[17] A. Hultqvist, M. Edoff, T. Törndahl, Evaluation of Zn–Sn–O buffer layers for $CuIn_{0.5}Ga_{0.5}Se_2$ solar cells, Prog. Photovolt. Res. Appl. 19 (2011) 478–481.
[18] A. Hultqvist, C. Platzer-björkman, U. Zimmermann, M. Edoff, T. Törndahl, Growth kinetics, properties, performance, and stability of atomic layer deposition Zn–Sn–O buffer layers for Cu(In,Ga)Se$_2$ solar cells, Prog. Photovolt. Res. Appl. 20 (2012) 883–891.
[19] J. Lindahl, C. Hägglund, J.T. Wätjen, M. Edoff, T. Törndahl, The effect of substrate temperature on atomic layer deposited zinc tin oxide, Thin Solid Films 586 (2015) 82–87.
[20] J. Kessler, M. Bodegård, J. Hedström, L. Stolt, Baseline Cu(In,Ga)Se$_2$ device production: control and statistical significance, Sol. Energy Mater. Sol. Cells 67 (2001) 67–76.
[21] J. Tauc, Optical properties and electronic structure of amorphous Ge and Si, Mater. Res. Bull. 3 (1968) 37–46.
[22] R.M. Langford, C. Clinton, In situ lift-out using a FIB-SEM system, Micron 35 (2004) 607–611.
[23] H. Field, UV–vis–IR spectral responsivity measurement system for solar cells, in: AIP Conference Proceedings, 1999, pp. 629–635.
[24] M. Burgelman, P. Nollet, S. Degrave, Modelling polycrystalline semiconductor solar cells, Thin Solid Films 361–362 (2000) 527–532.
[25] A. Klein, T. Löher, C. Pettenkofer, W. Jaegermann, Chemical interaction of Na with cleaved (011) surfaces of CuInSe$_2$, J. Appl. Phys. 80 (1996) 5039–5043.
[26] U. Rau, H.W. Schock, Electronic properties of Cu(In,Ga)Se$_2$ heterojunction solar cells – recent achievements, current understanding, and future challenges, Appl. Phys. A 69 (1999) 131–147.
[27] J. Jacobsson, T. Edvinsson, Photoelectrochemical determination of the absolute band edge positions as a function of particle size for ZnO quantum dots, J. Phys. Chem. C 116 (2012) 15692–15701.

[28] W.-S. Choi, Preparation of zinc-tin-oxide thin film by using an atomic layer deposition methodology, J. Korean Phys. Soc. 57 (2010) 1472–1476.
[29] D. Rudmann, A.F. Da Cunha, M. Kaelin, F. Kurdesau, H. Zogg, A.N. Tiwari, et al., Efficiency enhancement of Cu(In,Ga)Se_2 solar cells due to post-deposition Na incorporation, Appl. Phys. Lett. 84 (2004) 1129–1131.
[30] F. Pianezzi, P. Reinhard, A. Chirilă, B. Bissig, S. Nishiwaki, S. Buecheler, et al., Unveiling the effects of post-deposition treatment with different alkaline elements on the electronic properties of CIGS thin film solar cells, Phys. Chem. Chem. Phys. 16 (2014) 8843–8851.
[31] P. Salomé, A. Hultqvist, V. Fjällström, M. Edoff, B. Aitken, K. Vaidyanathan, et al., Cu(In,Ga)Se_2 solar cells with varying Na content prepared on nominally alkali-free glass substrates, IEEE J. Photovolt. 3 (2013) 852–858.
[32] C. Thompson, S. Hegedus, W. Shafarman, D. Desai, Temperature dependence of V_{OC} in CdTe and Cu(InGa)$(SeS)_2$-based solar cells, in: Proceedings of the 33rd IEEE PVSC Conference, 2008, pp. 2–7.
[33] S.S. Hegedus, W.N. Shafarman, Thin-film solar cells: device measurements and analysis, Prog. Photovolt. Res. Appl. 12 (2004) 155–176.
[34] U. Rau, P.O. Grabitz, J.H. Werner, Resistive limitations to spatially inhomogeneous electronic losses in solar cells, Appl. Phys. Lett. 85 (2004) 6010.
[35] V. Nadenau, U. Rau, A. Jasenek, H.W. Schock, Electronic properties of $CuGaSe_2$-based heterojunction solar cells. Part I. Transport analysis, J. Appl. Phys. 87 (2000) 584–593.
[36] S.-H. Wei, A. Zunger, Band offsets and optical bowings of chalcopyrites and Zn-based II–VI alloys, J. Appl. Phys. 78 (1995) 3846–3856.
[37] J. Malmström, J. Wennerberg, M. Bodegard, L. Stolt, Influence of Ga on the current transport in Cu(In,Ga)Se_2 thin film solar cells, in: Proceedings of the 17th European Photovoltaic Solar Energy Conference, 2001, pp. 1265–1268.
[38] M. Contreras, L. Mansfield, B. Egaas, J. Li, M. Romero, R. Noufi, et al., Wide bandgap Cu(In,Ga)Se_2 solar cells with improved energy conversion efficiency, Prog. Photovolt. Res. Appl. 20 (2012) 843–850.
[39] S. Siebentritt, What limits the efficiency of chalcopyrite solar cells? Sol. Energy Mater. Sol. Cells 95 (2011) 1471–1476.
[40] P. Jackson, D. Hariskos, R. Wuerz, O. Kiowski, A. Bauer, T.M. Friedlmeier, et al., Properties of Cu(In,Ga)Se_2 solar cells with new record efficiencies up to 21.7%, Phys. Status Solidi – Rapid Res. Lett. 9 (2015) 28–31.